



Entropy analysis of a solar-driven variable geometry ejector using computational fluid dynamics



Amir Omidvar, Mohsen Ghazikhani^{*}, Sayyed Mohammad Reza Modarres Razavi

Department of Mechanical Engineering, Ferdowsi University of Mashhad, P.O.B. 9177948944, Mashhad, Iran

ARTICLE INFO

Article history:

Received 31 October 2015

Received in revised form 23 March 2016

Accepted 30 March 2016

Keywords:

Variable geometry ejector

Entropy generation

Numerical simulation

ABSTRACT

In the present paper, a study of flow pattern in a variable geometry ejector used in solar refrigeration system was conducted in an effort to achieve the optimum geometry and improve the understanding of the important flow behaviors that lead to ejector performance drop. Since the entropy generation is equivalent to performance losses, this parameter was investigated in numerical simulations. The results showed that the mixing phenomenon act as a main role in the entropy generation when the temperature of the condenser is higher than critical temperature, meanwhile the shock event operates the major parameter when the condenser temperature is lower than critical. In addition, a remarkable correlation between the entropy generation and the ejector performance was revealed, and so 37% performance improvement obtained.

© 2016 Published by Elsevier Ltd.

1. Introduction

Nowadays, the demand for air-conditioning systems is rising due to the population growth and the improvement of life level. Air-conditioning systems mostly utilize electricity as the primary source of energy, that not environment-friendly option where fossil fuels are used to produce the electricity. Since a direct relationship exists between the rate of cooling and solar radiation, solar-driven cooling systems have been proposed as an effective method for reducing electricity consumption. Ejector refrigeration systems are a type of cooling system that work with solar energy. In recent years, researchers have paid special attention to ejector refrigeration systems due to their individual advantages such as simple structure, low initial expenses, low maintenance costs, and high durability because of the lack of moving parts. However, there are two main challenges in adopting these systems: low coefficient of performance (COP) and high sensitivity to operating conditions.

To overcome these drawbacks, many studies have been carried out using the first and second laws of thermodynamics. A review of recent achievements to improve the ejector refrigeration systems is done by Chen et al. [1]. Considerable efforts have been made to design of an optimal ejector from the first law viewpoint. This could be done by investigating the behavior of inner flow in ejectors using laser tomography [2–4] and numerical methods [5–8].

Various studies have been carried out to find the most accurate and capable method in predicting the ejector flow. Bartosiewicz et al. [9] compared the numerical results by laser tomography pictures provided by Desevaux's [2] and showed that $k-\omega$ -sst model has more accuracy to predict. del Valle et al. [10] also demonstrated that the pressure profiles computed by $k-\epsilon$ standard and $k-\omega$ -sst models have good agreement with experimental results. Sriveerakul et al. [11] showed that the realizable $k-\epsilon$ turbulence model is able to predict the flow behavior by measuring pressure distribution. Based on Schlieren approach Zhu and Jiang [4] proposed RNG $k-\epsilon$ as the best model for predictions of both the mass flow rate and shock wave structures. Gagan et al. [12] adopted PIV technique and concluded that results of the $k-\epsilon$ standard has the best consistency with experimental results. Moreover, some new papers about improving the ejector performance have been published [13,14].

However, besides the energy analysis of energy systems, the second law analysis (energy analysis) could be a tool to find the sources of energy loss in a system. In the case of ejector refrigeration systems like other energy devices, exergy analysis could help to ameliorate the system performance. Here a brief review is done of some studies on the exergy analysis of ejectors. Khennich et al. [15] used the temperature–enthalpy diagram to study the exergetic performance of an ejector refrigeration cycle. Using the diagram, they demonstrated the exergy losses in different components of the cycle such as pumps, turbines, compressors, expansion valves, condensers and evaporators. Chen et al. [16] investigated ejector performance characteristics in an ejector

^{*} Corresponding author.

E-mail address: ghazikhani@um.ac.ir (M. Ghazikhani).

refrigeration cycle with refrigerants R600a, R245fa and R141b. The amount of the primary and secondary flows superheating along with the operating temperatures of generator, evaporator and condenser were investigated as the external properties. Moreover, analytical expressions were presented for efficiency of diffuser, nozzle and mixing. The effect of the above characteristics on the amount of irreversibility generated in the ejector was also studied.

Arbel et al. [17] showed that ejector irreversibility was resulted from three factors including mixing, the kinetic energy losses and the normal shock wave. They disclosed that created irreversibilities by mixing and normal shock wave could be removed by applying appropriate conditions in the gas inlet section and using an adjustable throat respectively.

Chen et al. [18] conducted an investigation of an ejector refrigeration system using conventional and advanced exergy analysis. They also studied avoidable and unavoidable exergy destructions in each component of the system using water and refrigerant R245a as the working fluids. Their results showed that highest exergy destruction takes place in the ejector, accounting for 53.6% of the total system exergy destruction, followed by the generator (24.7%) and finally the condenser (15.9%). The exergy loss within the evaporator, throttling valve and pump, however, are minuscule compared to overall system exergy destruction. Sadeghi et al. [19] carried out an exergoeconomic analysis of ejector refrigeration cycle theoretically. They revealed that the generator has the highest exergy destruction followed by the ejector, albeit, under optimal conditions. It was also disclosed that the product unit cost in the ejector refrigeration systems is higher than absorption refrigeration systems, which is due to the lower second law efficiency of the ejector refrigeration system. More recently, Hakaki et al. [20] developed a CFD software to optimize the ejector configuration by entropy generation minimization approach. They could increase the entrainment ratio up to 29% by this method. However, it is very complicated to manufacture it due to adopting a parabolic primary nozzle in the ejector. Construction can become even more challenging when using refrigerants with high molecular weight such as R134a or R600a for small cooling capacity devices, because the size of primary nozzle shrinks.

According to Pridasawas and Lundqvist [21] who investigated the solar-driven ejector refrigeration cycle by exergy analysis, most of the exergy destruction occurs in solar collector, followed by the ejector. In addition, they disclosed that the irreversibility has an inverse relation with the evaporation temperature, which affects the total system irreversibility dramatically. It was also proven that an optimum generator temperature could be obtained for each evaporator temperature. Furthermore, among the analyzed solar collectors, evacuated-tube solar collector had the highest efficiency because of lower irreversibility levels.

Alexis [22] studied each of the components of the steam-ejector refrigeration system through exergy loss and coefficient of performance. The results showed that the ejector was the most responsible factor for exergy destruction of the system and the condenser was the next.

A review of the literature shows that there is no study on the optimization of an ejector with variable geometry by the entropy generation minimization method. Although, the overall irreversibility generated within the ejector has been estimated in most of studies, however the major causes of the irreversibility have been less discussed. The present research presents a deep analysis of flow processes and phenomena that lead to entropy generation in ejector. The optimum geometry and operating condition of the ejector are found using entropy generation analysis through a numerical approach. The relationship of entrainment ratio and entropy generation is investigated, and the roles of shock position and flow pattern in the entropy generation are explored.

2. Ejector refrigeration systems

As can be seen in Fig. 1, ejector refrigeration systems have been developed from conventional refrigeration system namely vapor compression. Instead of mechanical compressors, ejector is used to increasing pressure in the ejector refrigeration systems. In these systems, the evaporated refrigerant is compressed and then delivered to condenser by means of the ejector. Required heat energy for steam generation is usually provided with low temperature heat sources such as solar collectors.

A schematic of a typical ejector is shown in Fig. 2 This system consists of primary nozzle, mixing zone, throat and diffuser. Primary stream flowing from generator enters the ejector at high pressure and temperature, and speeds up to supersonic velocities by expanding through a converging-diverging nozzle. This supersonic stream makes a low pressure region which is formed at the nozzle exit plane (NXP). Thus, the secondary fluid flow can be entrained into the ejector. The primary stream applies shear stress to the secondary fluid. Therefore, the speed of the secondary stream rises up to sonic velocity. During this process, mixing of the two flows begins and the flows can be fully mixed by the end of the constant cross-section region. Depending on the condenser pressure, a shock occurs in a location between constant cross-section region and the beginning of the diffuser and pressure of the stream increases due to this event. Eventually the mixed stream exits from the ejector at the pressure that equals to condenser pressure.

In ejectors, the entrainment ratio is the most important characteristic that specifies its performance. Entrainment ratio (ω) is usually defined as the ratio of the secondary flow rate (\dot{m}_s) to the primary flow rate (\dot{m}_p):

$$\omega = \frac{\dot{m}_s}{\dot{m}_p} \quad (1)$$

The characteristic curve of an ejector, which shows its performance, is illustrated in Fig. 3. As shown in this figure, there are three different operating conditions for the ejector. The best operating regime takes place when the ejector works at critical condition that is also called “design condition”. Ejector works with maximum entrainment ratio in this condition. In all three operating conditions, primary mass flow rate is constant because the primary throat Mach number equal to one.

By increasing the back pressure, secondary mass flow rate decrease due to subsonic velocity and increasing pressure at mixing area. Besides, decreasing the back pressure choked constant area section too, double choking, and doesn't increase secondary mass flow rate. Complete discuss can find in [23].

3. Ejector design conditions

The ejector designed theoretically as a single phase constant-pressure mixing model described by He et al. [24]. The nominal cooling capacity was 750 W (≈ 1 hp) and isobutane used as refrigerant. According to hourly dynamic simulation conducted by Tash-touh et al. [25] evacuated tube solar collector is superior, so that generator temperature is considered up to 120 °C based on the results of Pridasawas and Lundqvist [21]. Evaporator and condenser temperatures have been considered 5 °C and 35 °C based on HVAC operating conditions and climatic conditions of the Middle East, respectively. More information is in Table 1.

Geometry variation of the ejector is achieved by changing the primary nozzle position. The zero position of the primary nozzle's outlet opening is considered at the beginning of the constant-area section with positive direction toward the inside of the ejector. Characteristic lengths and schematic of the ejector is shown in

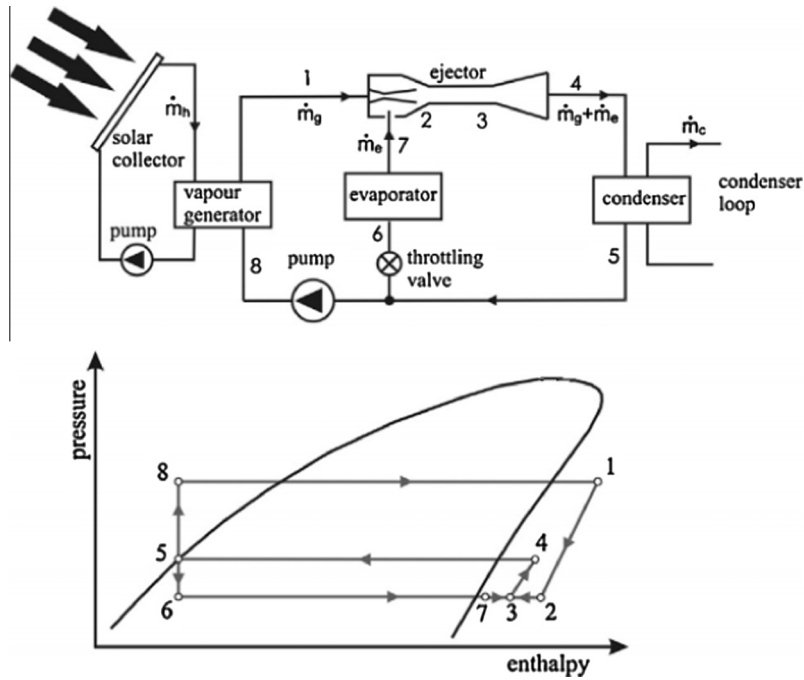


Fig. 1. Schematic ejector refrigeration cycle using solar energy heat source and its thermodynamic cycle.

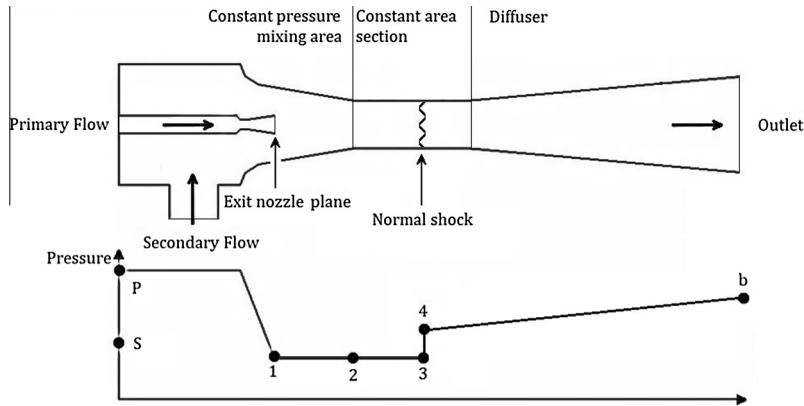


Fig. 2. Schematic of an ejector and pressure distribution inside it.

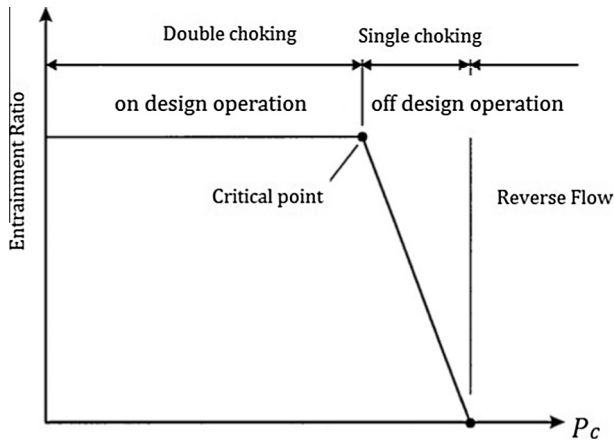


Fig. 3. Characteristic curve of an ejector for constant generator and evaporator pressures.

Table 1
Operating conditions of the ejector.

Evaporator capacity	Q_{eva}	750 W
Total pressure of primary stream	P_p	2634.13 kPa
Total temperature of primary stream	T_p	388 K
Total pressure of secondary stream	P_s	187.75 kPa
Total temperature of secondary stream	T_s	278 K
Total pressure of outlet stream	P_c	468.62 kPa
Total temperature of outlet stream	T_c	308 K

Figs. 4 and 5 respectively. Geometrical dimensions, which are listed in Table 2, are taken from the ejector that was manufactured for experiments.

4. CFD simulation

Numerical investigation has been carried out by means of Gambit 2.3 for mesh generation and Fluent 6.3.26 to solve the governing equations by control volume method.

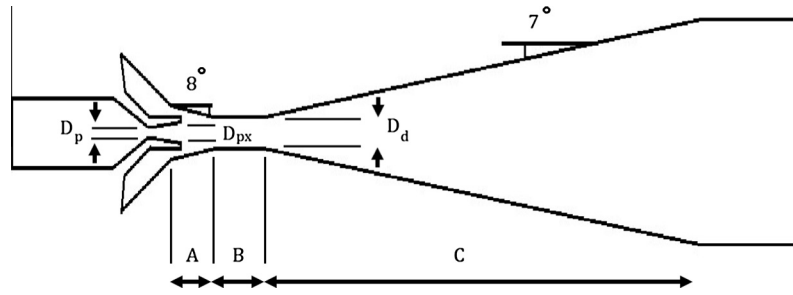


Fig. 4. Characteristic lengths of the ejector.

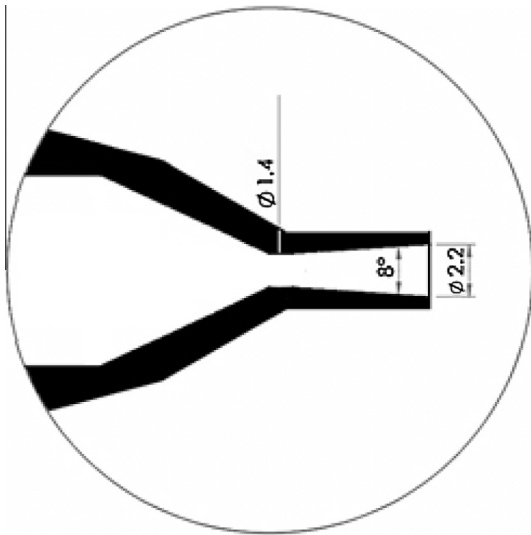


Fig. 5. Schematic of inside the primary nozzle (scale in mm).

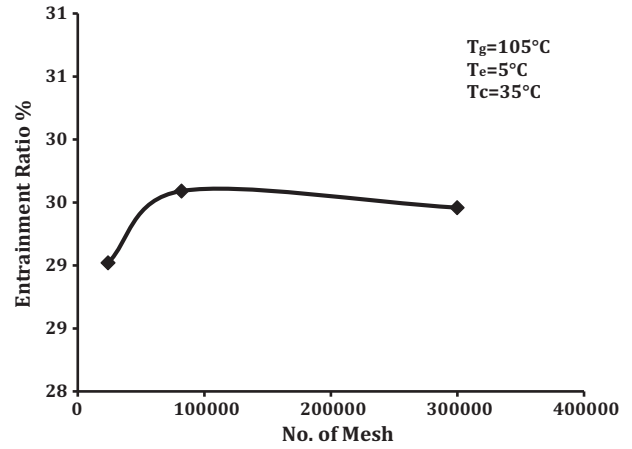


Fig. 7. Grid independency.

Table 2
Geometrical dimensions of the ejector.

Throat diameter of the primary nozzle	D_p	1.4 mm
Outlet opening diameter of the primary nozzle	D_{px}	2.2 mm
Diameter of the constant-area section	D_d	3.5 mm
Length of the constant-pressure mixing section	A	9 mm
Length of the constant-area section	B	9 mm
Length of the diffuser	C	88 mm

In order to reduce the calculations, instead of 3D domain with lots of cells, 2D axisymmetric computational domain has been preferred. Density-based method has been applied to solve the non-linear governing equations according to the compressibility of the flow. The Roe-FDS algorithm and the $k-\epsilon$ realizable model have been employed to solve the coupled pressure-velocity equations and flow turbulence respectively, and real gas properties used by FEQ Helmholtz equation of state for isobutane. In addition, the energy equation should be coupled with flow governing equations because of high velocity of the gas flowing through the ejector and the compressibility effects. Secondary mass flow rate was considered as the convergence criteria.

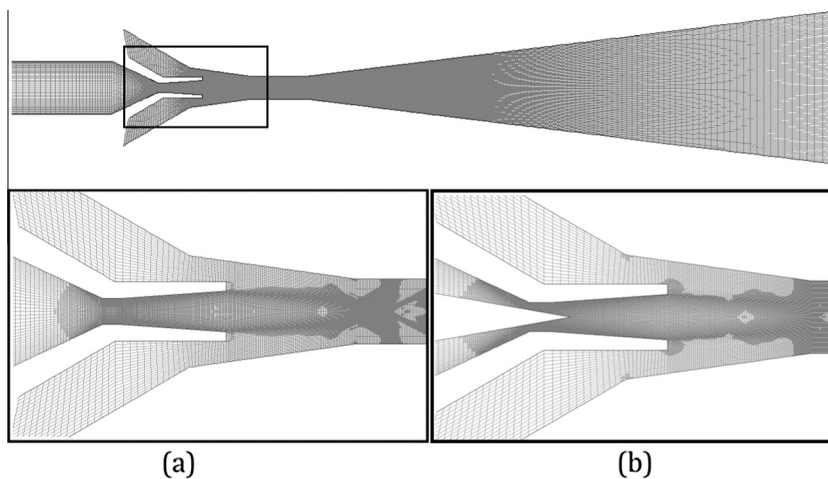


Fig. 6. Mesh structure and solution-adaptive refinement. (a) Without spindle and (b) with spindle.

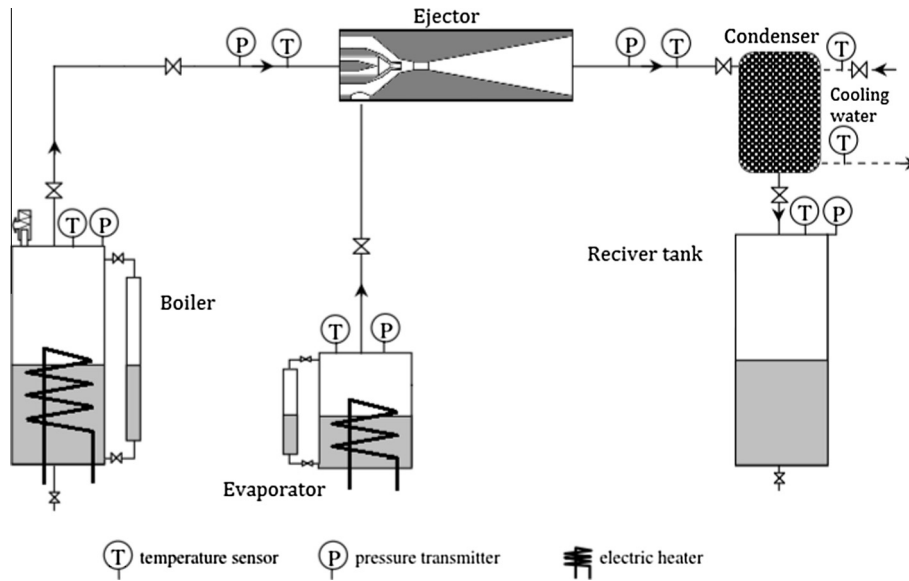


Fig. 8. Schematic diagram of experimental setup.



Fig. 9. A photograph of variable geometry ejector.

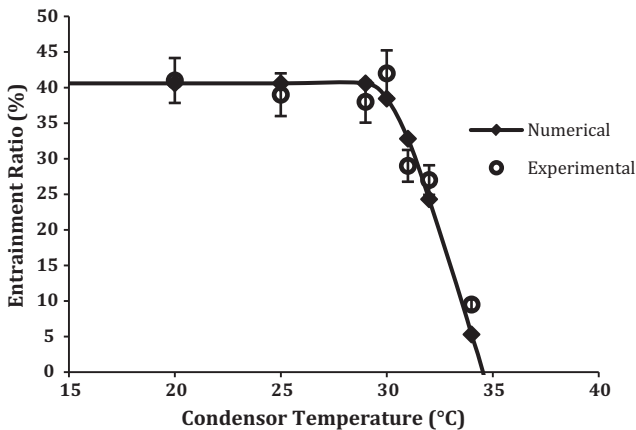


Fig. 10. Entrainment ratio as function of condenser temperature for numerical and experimental results.

Solving fluid flow and Helmholtz equation of state, all the specific properties of fluid including specific entropy obtain at each control volume. Total entropy calculates using surface integral at each section along the axis. The entropy generation calculated by entropy variation by two adjacent section along the axis.

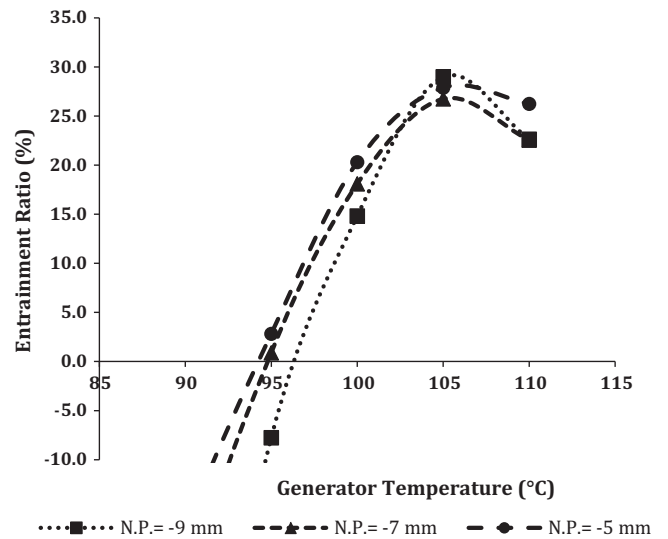


Fig. 11. Entrainment ratio at different generator temperatures and nozzle positions.

For the inlets and outlet of the flow, “pressure-out” boundary condition was applied with pressure and temperature values of each opening and all wall surfaces of the ejector were assumed adiabatic, because of thermal isolation and high flow velocity in the ejector, by applying a zero heat flux condition. Computational domain and grid system of the ejector are shown in Fig. 6. Grids adopted up to pressure difference between two near cells not be more than 10 Pa. The procedure give acceptable grid independency as shown in Fig. 7.

It is worth mentioning that the expansion process does not lead to condensation of the gas inside the constant-pressure zone and the flow remains single-phase because the slope of the saturated-vapor line is positive on the T-s diagram of isobutene.

5. Experimental validation

In order to validate the numerical simulation, the results were compared with experiments results for entrainment ratio. For this

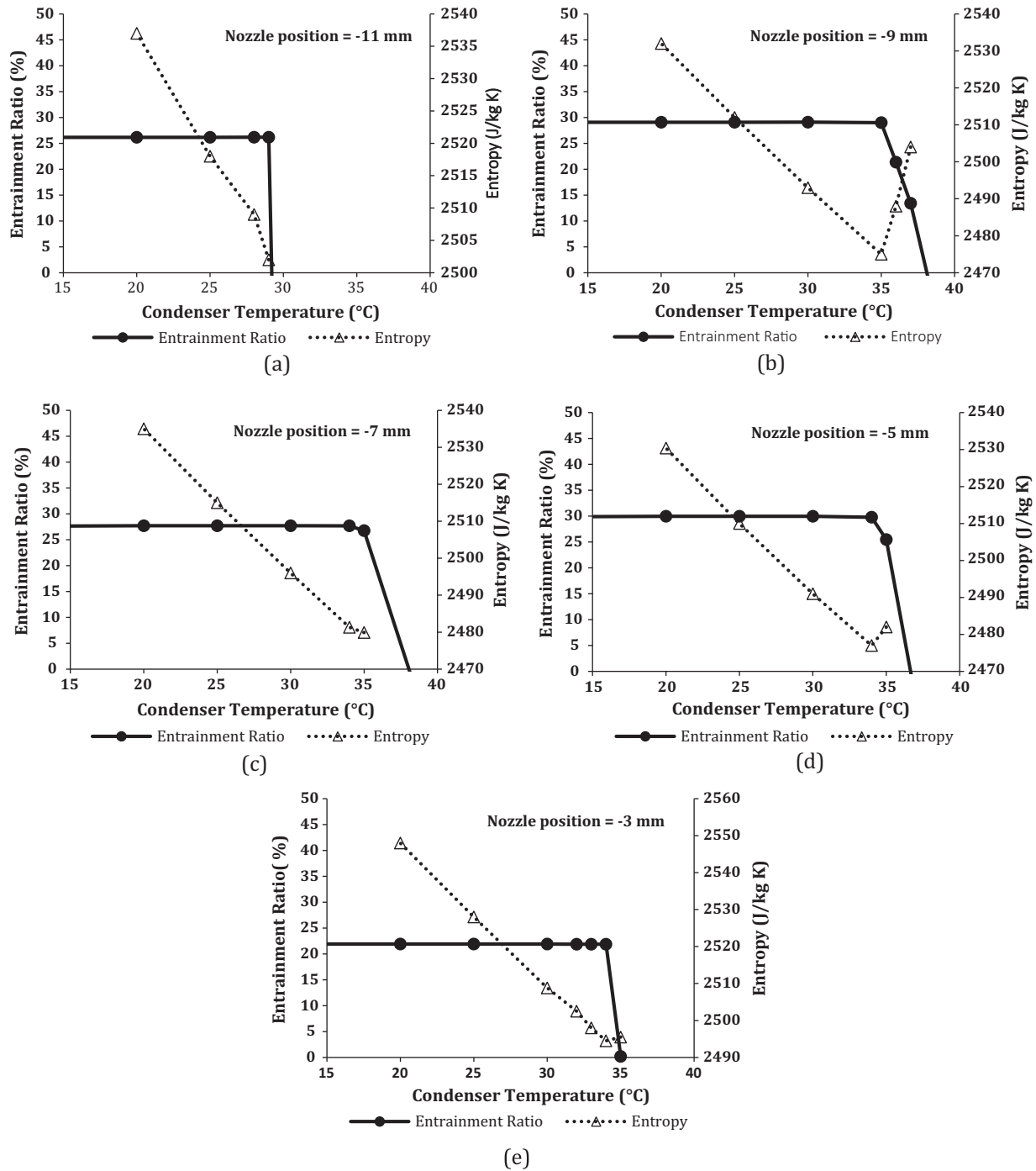


Fig. 12. Ejector performance at generator 105 °C and evaporator 5 °C, (a) nozzle position = -11 mm, (b) nozzle position = -9 mm, (c) nozzle position = -7 mm, (d) nozzle position = -5 mm, (e) nozzle position = -3 mm.

purpose, a test section has been developed using R600a as the refrigerant. The schematic figure has been presented in Fig. 8. The main components comprising the test section are boiler, condenser, ejector, condensate receiver tank, and evaporator. Here a variable geometry ejector was used, capable of adjusting the nozzle exit position (NXP) and altering the ratio of the primary throat area against the ejector throat area (Fig. 9). This was possible due to utilizing a spindle in the primary nozzle. This design makes it possible to independently adjust geometrical parameters. Since various parts of the ejector are movable, two O-rings have been implemented for sealing each connection. A 4 kW electrical heater is used in the boiler as the heat source, which controls the pressure

and temperature. Another electrical heater (1 kW) is implemented for the evaporator. As the primary nozzle operate in choking condition, mass flow rate was evaluated by choked flow equations in the primary throat. The secondary mass flow rate was determined by measuring the refrigerant liquid level in the evaporator, using attached sight glass in steady operation. A plate heat exchanger was utilized as the condenser and the coolant flow rate regulates its temperature. This coolant flows from a huge receiver tank with constant temperature during the test. All components, including boiler, evaporator, and pipes are insulated to minimize heat loss. PT100 temperature sensors and pressure transducers were applied by 0.1 °C and 0.5% of full-scale accuracy respectively.

A data logger saved all measurements every 5 s in a text file, transferring them to an MS Excel file after test completion. The uncertainty calculated for mass entrainment ratio was 7.7%. A Comparison was made on the following conditions: 5 °C evaporator temperature, 95 °C generator and without spindle in the primary nozzle. Fig. 10 shows the variation of the entrainment ratio at different back pressures from both numerical and experimental results. Reasonable agreement between the results is an indication of the CFD model's ability to predict the flow behavior within the ejector.

6. Results and discussion

6.1. Entropy variation

Primarily, the generator temperature was selected by analyzing ejector performance at nozzle positions –9, –7 and –5 mm. For the purpose, evaporator and condenser temperatures are 5 °C and 35 °C respectively according to operating design conditions. As shown in Fig. 11, in all evaluated nozzle positions, entrainment ratio reaches to its maximum value at 105 °C. In fact, increase in pressure and temperature of the generator provides more energy for entraining the secondary flow from the evaporator. This procedure continues until more increase of the primary flow does not result in the increase of the secondary flow and even decreases it.

According to the results, generator temperature of 105 °C has been considered to investigate the ejector performance in different primary nozzle positions and at different condenser temperatures and also the outlet entropy of the ejector has been calculated in all of these simulations. The entropy at each section was calculated by area-weighted summation along the local diameter. As it can be seen in Fig. 12, minimum output entropy occurs at ejector critical point for all primary nozzle positions. Results clearly shows a coincidence between entrainment ratio and entropy generation that both parameters have their optimum values in the critical point. Fig. 13 shows that minimum entropy generation takes place at nozzle positions of –5 and –9, which is in agreement with maximum entrainment ratio. According to the performance curve of the ejector, although increase of condenser temperature up to critical point does not make any change in entrainment ratio, outlet entropy decreases until it reaches to its minimum value in the critical point. Further decrease of the condenser temperature causes more entropy generation and correspondingly ejector performance drops dramatically. Based on the aforementioned results, output entropy value can be used as a criterion to obtain the optimal

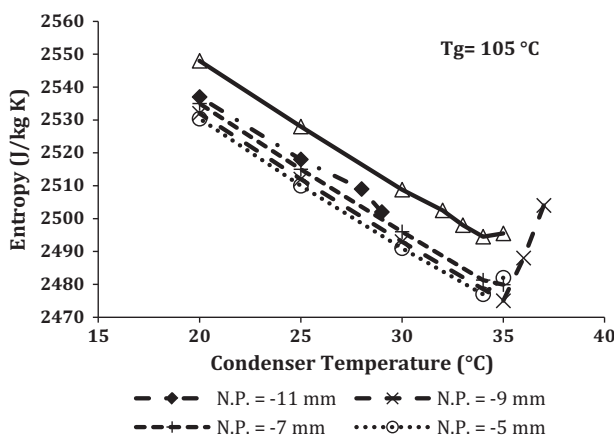


Fig. 13. Entropy variation at generator 105 °C and evaporator 5 °C.

performance of the ejector. The results show that an ejector with variable primary nozzle can improve the performance of solar refrigeration system along the day.

6.2. Flow analysis in the ejector

Fig. 14 shows the entropy variation along the ejector for nozzle position –9 mm and generator temperature 105 °C. In addition, to find out the correlation between shock waves and entropy generation along the ejector, several Mach number contours for the values greater than one are shown in Fig. 15. Fig. 14 shows in all condenser temperatures there are two entropy generation mechanisms. The entropy generation is starting at the primary nozzle exit plane. As the mixing process becomes completed, entropy generation reduces. The entropy increment of the mixing process can be seen in the constant-pressure region. The second source of irreversibility, that is stronger at lower condenser temperatures, is shock phenomenon. As it can be seen in Fig. 14, as the flow passes through a shock wave, a large entropy variation occurs.

The critical point is the point at which sum of the entropy generation caused by two mentioned mechanisms becomes minimum. For the given generator an evaporator temperatures and nozzle position the critical point is at the condenser temperature of 35 °C. In addition, the results demonstrate that the mixing process is completed at a location where the last shock occurs.

At the lower condenser temperature (20, 25 and 30 °C), the major factor causing entropy generation is chok. The lower condenser temperature the strongest shock and grater entropy generation. Comparison between Figs. 14 and 15 shows entropy varies as long as the Mach number is greater than unity. In other words, by neglecting the viscous effects, after the shock there is no significant entropy variation.

As the results show, at lower condenser temperatures, supersonic flow penetrates more into the diffuser, and a stronger shock occurs later. At condenser temperature 20 °C there is longest shock wave and strongest shock. Consequently, the stronger shock results in more entropy generation in the flow field. By increasing the condenser temperature up to 35 °C, shock occurs closer to the primary nozzle exit position and the entropy generation process begins earlier too. However, outlet entropy is greater than critical one.

The presented results in Fig. 12 shows that the critical point is at the condenser temperature of 35 °C, and it can be seen from Fig. 14 that minimum generated entropy of mixing and shock wave

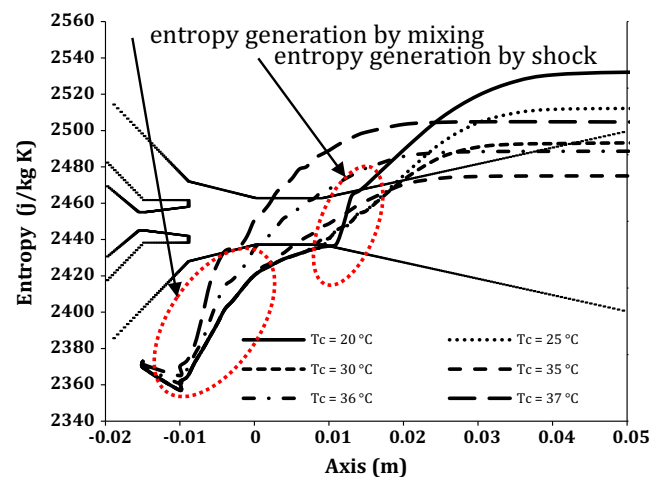


Fig. 14. Entropy variation along the ejector in primary nozzle position –9 mm and generator temperature of 105 °C.

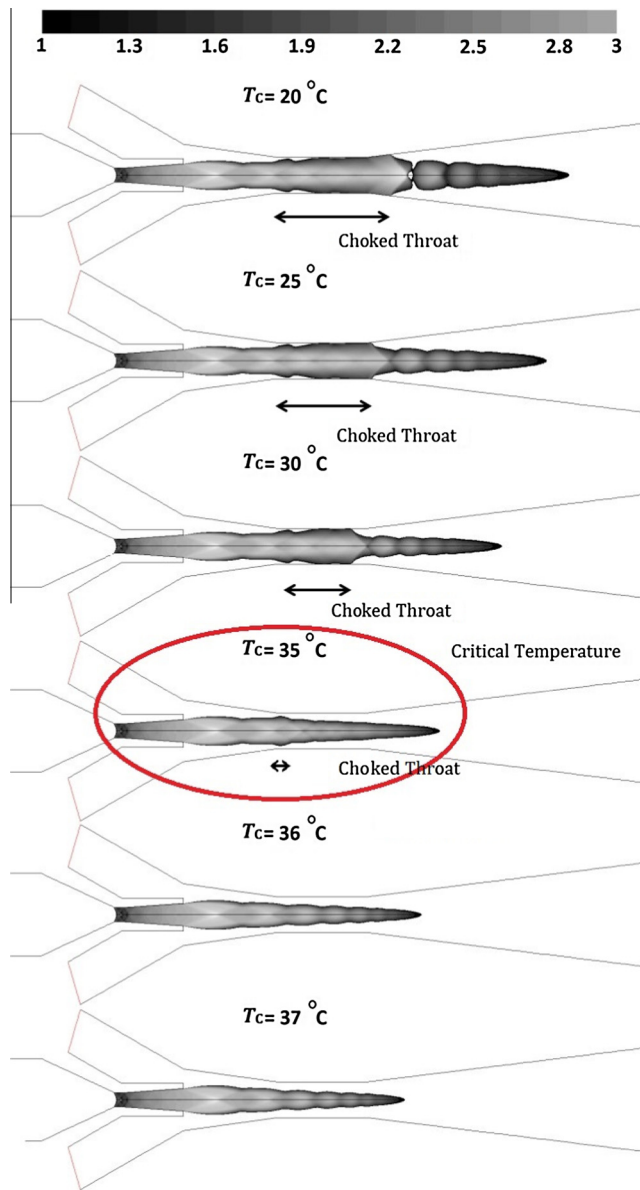


Fig. 15. Mach contours for different condenser temperature along the ejector in primary nozzle position -9 and generator temperature of 105°C .

occurs at the same condenser temperature. This coincidence shows a remarkable correlation between the optimum operating conditions and minimum total entropy generation.

A closer look into Fig. 15 reveals that at condenser temperature lower than critical temperature, the flow in the constant-area section is sonic or supersonic. An increase results in a smaller length of the constant-area section in which $Ma \geq 1$ throughout the cross section (choked Throat). The decrease in this length caused by back pressure increase continues until at the critical back pressure, choked throat is minimum. In fact, the optimum flow conditions exist when the flow is choked at only one cross section of the constant-area section.

7. Conclusion

In this paper for the first time, entropy generation analysis is implemented to obtain the optimum the nozzle position in a vari-

able geometry ejector used in solar refrigeration systems using outlet entropy as optimization criteria.

The main findings of this study can be summarized as follow:

- A deep study of performance drop in the ejector was performed.
- The optimum primary nozzle position was at -5% and 37% performance improvement obtained.
- The entropy generation is correlated with the entrainment ratio and ejector performance. Therefore, it can be a significant factor in studying and optimizing the operating conditions and geometrical parameters of the ejector.
- The entropy generation is mainly caused by two factors: mixing and shock. When the condenser temperature is below the critical temperature, shock phenomenon has a more significant effect on entropy generation. However, at temperatures higher than the critical point, mixing effect is the more important.
- In order to optimize the ejector geometry, the position of entropy generation needs to be investigated along the ejector, in the constant pressure section to improve the mixing and in the constant-area section to reduce the shocks.
- In addition, when condenser works at a critical point temperature, the total amount of entropy generation caused by the two factors and the outlet entropy generation will be concluded to be minimal.

Acknowledgement

We hourly appreciate Khorasan Razavi Gas Co. for their technical and financial support of this research.

References

- [1] Chen X, Omer S, Worall M, Riffat S. Recent developments in ejector refrigeration technologies. *Renew Sustain Energy Rev* 2013;19:629–51.
- [2] Desevaux P, Mellal A, Alves de Sousa Y. Visualization of secondary flow choking phenomena in a supersonic air ejector. *J Visual* 2004;7(3):249–56.
- [3] Zhu Y, Jiang P. Experimental and analytical studies on the shock wave length in convergent and convergent–divergent nozzle ejectors. *Energy Convers Manage* 2014;88:907–14.
- [4] Zhu Y, Jiang P. Experimental and numerical investigation of the effect of shock wave characteristics on the ejector performance. *Int J Refrig* 2014;40:31–42.
- [5] Allouche Y, Bouden C, Varga S. A CFD analysis of the flow structure inside a steam ejector to identify the suitable experimental operating conditions for a solar-driven refrigeration system. *Int J Refrig* 2014;39:186–95.
- [6] Chandra VV, Ahmed MR. Experimental and computational studies on a steam jet refrigeration system with constant area and variable area ejectors. *Energy Convers Manage* 2014;79:377–86.
- [7] Pianthong K, Seehanam W, Behnia M, Sriveerakul T, Aphornratana S. Investigation and improvement of ejector refrigeration system using computational fluid dynamics technique. *Energy Convers Manage* 2007;48:2556–64.
- [8] Chong D, Hu M, Chen W, Wang J, Liu J, Yan J. Experimental and numerical analysis of supersonic air ejector. *Appl Energy* 2014;130:679–84.
- [9] Bartosiewicz Y, Aidoun Z, Desevaux P, Mercadier Y. Numerical and experimental investigations on supersonic ejectors. *Int J Heat Fluid Flow* 2005;26(1):56–70.
- [10] del Valle J García, Sierra-Pallares J, Carrascal P García, Ruiz F Castro. An experimental and computational study of the flow pattern in a refrigerant ejector. Validation of turbulence models and real-gas effects. *Appl Therm Eng* 2015;89:795–811.
- [11] Sriveerakul T, Aphornratana S, Chunnanond K. Performance prediction of steam ejector using computational fluid dynamics: Part 1. Validation of the CFD results. *Int J Therm Sci* 2007;46:812–22.
- [12] Gagan J, Smierciew K, Butrymowicz D, Karwacki J. Comparative study of turbulence models in application to gas ejectors. *Int J Therm Sci* 2014;78:9–15.
- [13] Chen W, Chen H, Shi C, Xue K, Chong D, Yan J. A novel ejector with a bypass to enhance the performance. *Appl Therm Eng* 2016;93:939–46.
- [14] Opgenorth MJ, Sederstrom D, McDermott W, Lengsfeld CS. Maximizing pressure recovery using lobed nozzles in a supersonic ejector. *Appl Therm Eng* 2012;37:396–402.
- [15] Khennich M, Sorin M, Galanis N. Equivalent temperature–enthalpy diagram for the study of ejector refrigeration systems. *Entropy* 2014;16(5):2669–85.
- [16] Chen J, Havtun H, Palm B. Parametric analysis of ejector working characteristics in the refrigeration system. *Appl Therm Eng* 2014;69(1–2):130–42.

- [17] Arbel A, Shklyar A, Hershgal D, Barak M, Sokolov M. Ejector irreversibility characteristics. *J Fluids Eng* 2003;125(1):121–9.
- [18] Chen J, Havtun H, Palm B. Conventional and advanced exergy analysis of an ejector refrigeration system. *Appl Energy* 2015;144:139–51.
- [19] Sadeghi M, Mahmoudi SMS, Saray R Khoshbakhti. Exergoeconomic analysis and multi-objective optimization of an ejector refrigeration cycle powered by an internal combustion (HCCI) engine. *Energy Convers Manage* 2015;96:403–17.
- [20] Hakkaki-Fard A, Aidoun Z, Ouzzane M. A computational methodology for ejector design and performance maximisation. *Energy Convers Manage* 2015;105:1291–302.
- [21] Pridasawas W, Lundqvist P. An exergy analysis of a solar-driven ejector refrigeration system. *Sol Energy* 2004;76(4):369–79.
- [22] Alexis GK. Exergy analysis of ejector-refrigeration cycle using water as working fluid. *Int J Energy Res* 2005;29:11.
- [23] Besagni G, Mereu R, Inzoli F. Ejector refrigeration: a comprehensive review. *Renew Sustain Energy Rev* 2016;53:373–407.
- [24] He S, Li Y, Wang RZ. Progress of mathematical modeling on ejectors. *Renew Sustain Energy Rev* 2009;13:1760–80.
- [25] Tashtoush B, Alshare A, Al-Rifai S. Hourly dynamic simulation of solar ejector cooling system using TRNSYS for Jordanian climate. *Energy Convers Manage* 2015;100:288–99.